MODIFICATION OF HAIRPIN AUTO-GENERATION PROCESS IN TURBULENT CHANNEL FLOWS DUE TO POLYMER STRESS

Kyoungyoun Kim
Department of Mechanical Engineering
Hanbat National University
Daejeon 305-719, South Korea
kkim@hanbat.ac.kr

R. Sureshkumar
Department of Biomedical and Chemical Engineering, Department of Physics
Syracuse University
Syracuse, NY 13244, USA
rsureshk@syr.edu

ABSTRACT

To study the influence of dynamical interactions between turbulent vortical structures and polymer stress on turbulent friction drag reduction, a series of simulations were performed for channel flow at Re_τ =395. The initial eddy extracted by the conditional averages for the Q2 event from fully turbulent Newtonian flow is self-consistently evolved in the presence of polymer stresses by utilizing the FENE-P model (finitely extensible nonlinear elastic-Peterlin). The initial polymer conformation fields are given by the solutions of FENE- P model equations for the Newtonian mean shear. For a relatively low Weissenberg number, defined as the ratio of fluid relaxation time to the time scale of viscous diffusion, (We_τ = 50) the generation of new vortices is inhibited by polymer-induced counter torques, which results in fewer vortices in the buffer layer. However, the head of primary hairpin is unaffected by the polymer stress. For larger values of $We_\tau (\geq 100)$, the hairpin head becomes weaker and vortex auto-generation and Reynolds stress growth are almost entirely suppressed.

INTRODUCTION

It has been known for over six decades that the dissolution of minute amounts of high molecular weight polymers in wall-bounded turbulent flows results in a dramatic reduction in turbulent skin friction by up to 70% (Toms, 1948; Toms, 1977). The turbulent skin friction is closely related to the near-wall vortical structures in the inner layer and the outer layer hairpin vortices (Adrian, 2007; Robinson, 1991). However, the dynamical interactions between the coherent structures and polymer conformation (stress) field resulting in DR have remained relatively unexplored.

Recently, we have examined such interactions via dynamical simulations that track the evolution of hairpin vortices, i.e., counter-rotating pairs of quasi-streamwise vortices whose nonlinear auto-generation and growth, decay and breakup are centrally important to turbulence stress production (Kim et al., 2008a). It was shown that the auto-generation of new vortices is suppressed by the polymer stress, thereby decreasing the turbulent drag. In the dynamical simulations, the initial condition for the polymer conformation ($\mathbf{c} \equiv \langle \mathbf{qq} \rangle$, average second moment of the polymer chain end-to-end distance vector $\mathbf{q}$) is $\mathbf{c}(t = 0) = \mathbf{I}$, modeling a condition in which coiled polymers are suddenly introduced into the flow homogeneously. In the evolution of hairpin vortices, the initially coiled polymers start to be stretched by the mean shear of the initial flow field as well as fluctuating velocities due to the initial vortex. It was observed that within a time scale comparable to the polymer relaxation time, the coiled polymers stretched enough to affect the flow field.

In the present study, we have focused on the response time scales of polymers to fluctuating velocities associated with the turbulent vortical motions. Toward this end, we have imposed the initial polymer conformation fields corresponding to fully stretched polymers by the mean shear. The effect of dynamical interactions between turbulent vortical structures and polymer stress on turbulent friction drag reduction is examined by performing a series of simulations for channel flow at Re_τ = 395. The initial vortical structure extracted from fully turbulent Newtonian flow is self-consistently evolved in the presence of polymer stresses by utilizing the FENE-P (finitely extensible nonlinear elastic-Peterlin) model, as done in our earlier studies (Kim et al., 2008a; Kim et al., 2007).

NUMERICAL METHODS

In the present study, the evolution of an initially isolated vortical structure in the viscoelastic flow is tracked by performing a dynamical simulation of the channel flow where the polymer stress is modeled by the FENE-P model. The non-dimensional governing equations of unsteady, incompressible, viscoelastic flow with the FENE-P model are given by:

$$\nabla \cdot \mathbf{u} = 0 , \qquad (1)$$

$$\frac{\partial \mathbf{u}}{\partial t} + \mathbf{u} \cdot \nabla \mathbf{u} = -\nabla p + \frac{\beta}{\mathrm{Re}_\tau} \nabla^2 \mathbf{u} + \frac{1-\beta}{\mathrm{Re}_\tau} \nabla \cdot \boldsymbol{\tau} , \quad (2)$$

$$\frac{\partial \mathbf{c}}{\partial t} + \mathbf{u} \cdot \nabla \mathbf{c} = \mathbf{c} \cdot \nabla \mathbf{u} + \left(\nabla \mathbf{u} \right)^T \cdot \mathbf{c} - \boldsymbol{\tau} , \qquad (3)$$

where $\mathbf{u}$ is the velocity, p is the pressure, and $\boldsymbol{\tau} = ([L^2\text{-}3]/(L^2\text{-}tr(\mathbf{c}))\mathbf{c}\text{-}\mathbf{I})/(We_\tau/Re_\tau)$ is the polymer stress. The friction velocity u_τ ($= \tau_w/\rho$) and the channel half-height h are used as the velocity and length scale, respectively. Here, τ_w is the wall shear stress and ρ is fluid density, The Reynolds number is defined as $Re_\tau = u_\tau h/\nu_0$, where ν_0 is the zero shear-rate kinematic viscosity of the solution. The parameter β is the ratio of the solvent viscosity (μ_s) to the total solution zero-shear-rate viscosity (μ_0). The polymer stress $\boldsymbol{\tau}$ is obtained by solving an evolution equation for the conformation tensor $\mathbf{c}$, which is the average second moment of the polymer chain end-to-end distance vector ($\mathbf{q}$). The Weissenberg number $We_\tau = \lambda u_\tau^2/\nu_0$ is the ratio of the polymer relaxation time λ, to the flow time scale based on the friction velocity.

The initial condition for the velocity fields are given by the conditionally averaged flow fields associated with Reynolds stress producing events from the DNS data of fully developed Newtonian turbulent channel flow at $Re_\tau = 395$ (Kim et al., 2008b):

$$\mathbf{u}(\mathbf{x}, t = 0) = \overline{\mathbf{u}}(y) + \left\langle \mathbf{u}'(\mathbf{x}) \mid \mathbf{u}'(y_m) = \alpha(u_m, v_m, 0) \right\rangle$$

where the overbar denotes a time average. The events (u_m, v_m) are found from the maximum value of the probability weighted Reynolds shear stress $u'v'$ pdf(u',v'). The amplification factor (α) is referred to here as the strength of the Q2 event.

The initial polymer conformation field is given by the solutions of FENE-P model equations for the mean shear flow in the Newtonian case (Sureshkumar et al., 1997):

$$C_{xx}^{MF} = \frac{1}{F(y)} \left\{ 1 + \frac{2We_h^2}{F(y)^2} \left(\frac{dU}{dy} \right)^2 \right\} ,$$

$$C_{xy}^{MF} = \frac{We_h}{F(y)^2} \frac{dU}{dy} ,$$

$$C_{yy}^{MF} = C_{zz}^{MF} = \frac{1}{F(y)} ,$$

$$C_{xz}^{MF} = C_{yz}^{MF} = 0 ,$$

$$F(y) = \frac{\sqrt{3}\Omega(y)}{2\sinh(\phi/3)} ,$$

$$\Omega(y) = \frac{\sqrt{2}We_h}{L} \frac{dU}{dy} ,$$

$$\phi = \sinh^{-1}\left(3\sqrt{3}\Omega/2 \right) ,$$

where L is the maximum extensibility of the polymer molecules and $We_h = \lambda u_\tau/h$.

Time-integration of the governing equations is achieved by a semi-implicit method. For spatial derivatives, a spectral method is used with Fourier representations in the streamwise and spanwise directions, and Chebyshev expansion in the wall-normal direction. Periodic boundary conditions are applied in the streamwise and spanwise directions, and the no-slip boundary condition is imposed on velocity at the solid walls. The domain size is $4\pi h \times 2h \times \pi h$ in the streamwise, wall-normal, and spanwise directions, respectively. After tests of several grid resolutions, $256 \times 128 \times 192$ spectral modes are used, which results in Δx^+=19.4, Δy^+=0.12~9.69, and Δz^+=6.46.

RESULTS AND DISCUSSION

Figure 1 shows several snapshots of the evolution of initial vortical structure in the viscoelastic flows at different Weissenberg numbers (We_τ = 50, 100 and 200), where the vortices are identified by using the swirling strength (Zhou et al., 1999). The initial vortex was extracted by the Q2 event of α = 3 specified at y^+ = 50 from the Newtonian flow. The other rheological parameters of FENE-P model were selected as β = 0.9 and L = 120.

The evolution of initial vortex in the Newtonian flow is also displayed in Fig. 1(a) for the comparison. The initial vortical structure is changed to an Ω-shaped vortex (t^+ = 79) by the self-induced motion toward the bi-normal direction due to the local effect of the curved vortex line (Zhou et al., 1999). The secondary hairpin vortex (t^+ = 158) is generated upstream of the primary hairpin vortex and the vortices move downstream with almost the same convection velocity and little dispersion, forming a vortex packet. As time proceeds further, generation of new vortices in the buffer layer is also observed upstream of the secondary vortices.

In the viscoelastic flows, it is clearly observed that the auto-generation of new vortices is weakened. For a relatively low Weissenberg number (We_τ = 50) the generation of new vortices is inhibited due to polymer stress, which results in fewer vortices in the buffer layer. However, the head of
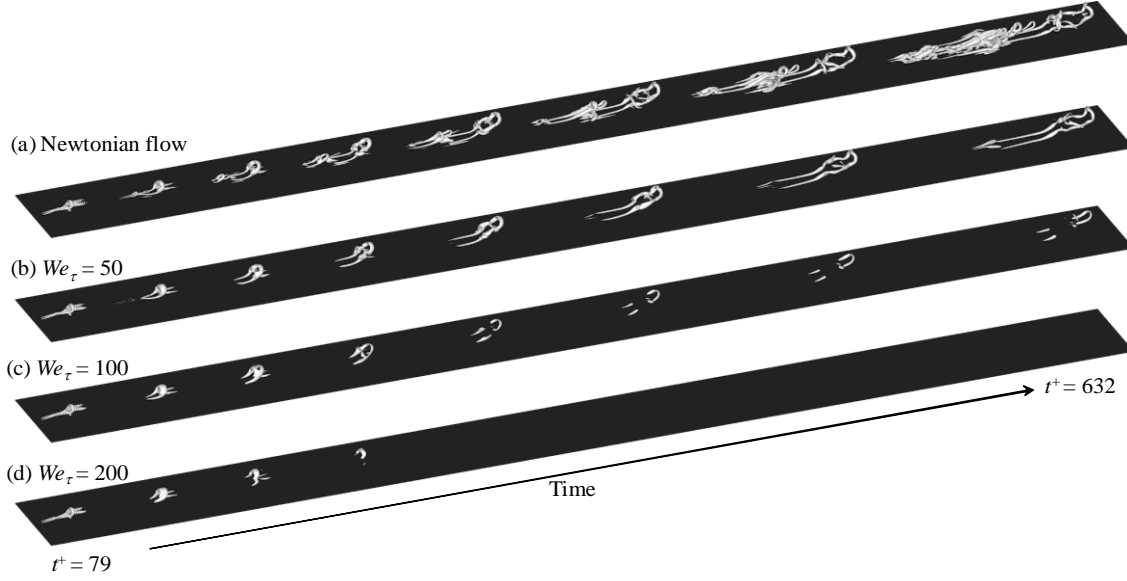
Fig. 1 Snapshots of the evolution of initial vortical structure extracted by Q2 event vector of strength $\alpha = 3$ specified $y^+ = 50$ from the Newtonian flow in (a) the Newtonian and (b)-(d) viscoelastic flows. Vortices are visualized by means of the iso-surfaces of 20% of the maximum swirling strength (λ_{ci}) of the initial eddy.

primary hairpin is unaffected by the polymer stress. For larger values of We_τ (≥ 100), the hairpin head becomes weaker as well as hairpin legs and vortex auto-generation is almost entirely suppressed.

Figure 2a shows the volume-averaged Reynolds shear stress normalized with respect to its initial value during the evolution of the initial vortex. The growth rate of the volume-averaged Reynolds shear stress decreases as We_τ increases due to the inhibited auto-generation mechanism and weakened vortices (Fig. 1). Further, a closer examination reveals that the viscoelastic effects manifest faster as the Weissenberg number increases. More than 5% deviation of Reynolds shear stress for the viscoelastic flows from the Newtonian flow begins at t^+ = 163, 122 and 98 for We_τ = 50, 100 and 200, respectively. In fully turbulent drag-reduced flows, lower values of Reynolds shear stress compared with the Newtonian flows are attributed to the weakened vortices because the polymer torque due to the polymer stress acts against the vortical motion of the near-wall vortices (Kim et al., 2007).

Figure 2b shows temporal evolution of the volume-averaged polymer torque magnitude. Polymer torque is defined as the curl of polymer force vectors:

$$\mathbf{T}_p = \nabla \times \mathbf{f}_p = \nabla \times \left(\frac{1-\beta}{\mathrm{Re}_\tau} \nabla \cdot \boldsymbol{\tau} \right)$$

Due to the initially stretched polymers by the mean shear, polymer torque starts to affect the flow from the early stages of the vortex evolution. The polymer torque magnitude increases as We_τ increases, which suggests higher We_τ induces larger polymer torque against the vortical motions and
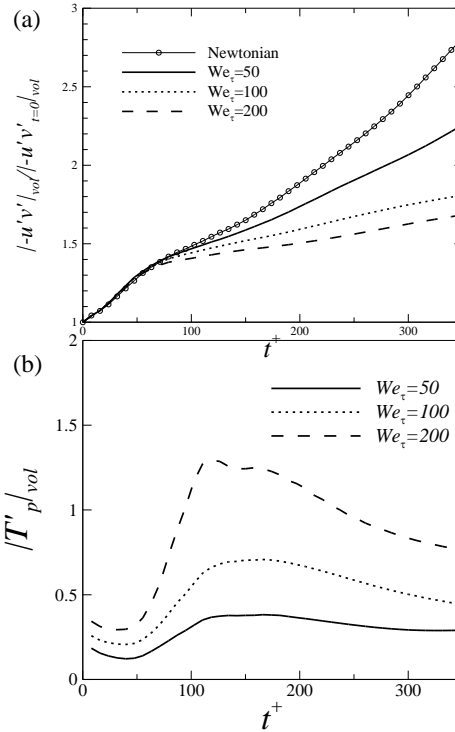
Fig. 2 Growth rate of volume-averaged values during evolution of the initial structure extracted by Q2 event vector of strength $\alpha = 3$ specified y^+=50 in the Newtonian flow. (a) Reynolds shear stress; (b) Polymer torque (magnitude).

3
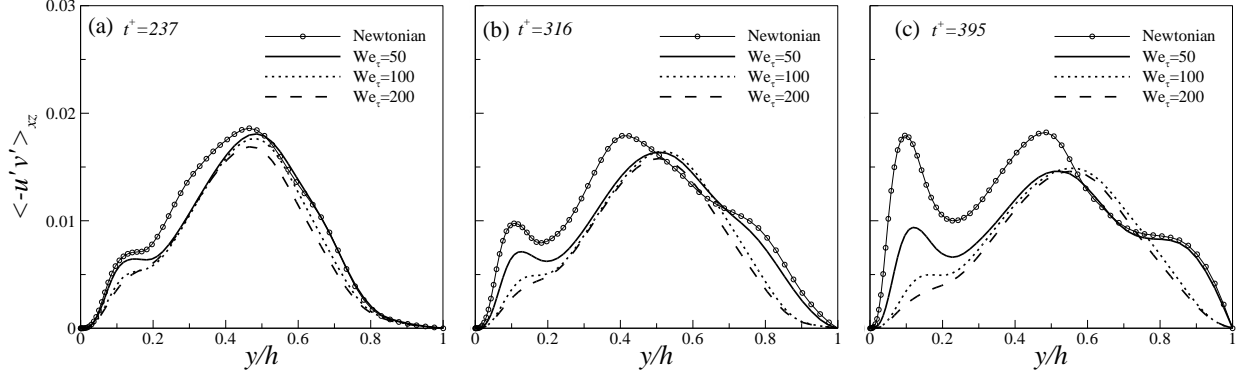
Fig. 3 Profiles of Reynolds shear stress during evolution of the initial structure extracted by Q2 event vector of strength $\alpha = 3$ specified at $y^+=50$ in the Newtonian flow.

thus greater weakening of the vortices. Regarding temporal variations of the polymer torque, they slightly decrease during earlier evolution ($t^+ < 50$) and then increase and decrease again ($t^+ > 200$). During the initial period with decrease of polymer torque, polymer torque is concentrated on the initial vortex which develops to Ω-shaped vortex. Around $t^+ = 100$, the polymer torque reaches its maximum value and this time corresponds to the generation of the secondary vortex upstream of primary hairpin in the Newtonian flow. This large polymer torque inhibits the auto-generation in the viscoelastic flows by weakening the vortical motions of the primary hairpin. The polymer torque decreases after $t^+ \approx 200$, which is attributed to the decrease in the vorticity magnitude after auto-generation since the weakened vortices induce less polymer stretching and thus weaker polymer torque.

Figure 3 shows the profiles of Reynolds shear stress averaged in the horizontal (x-z) plane. The Reynolds shear stress profile is shown to be closely related with the vortex evolution. In the Newtonian flow, at $t^+ = 237$, a local maximum located near the wall ($y/h = 0.1$) is observed, which is associated with new vortices generated upstream of the primary hairpin. The outer peak at $y/h \approx 0.45$ corresponds to the head of primary hairpin vortex. As time progresses, the secondary vortex head is lifted upward due to the Q2 pumping induced by the primary hairpin vortex and the lifted secondary hairpin head gives additional contribution to the Reynolds shear stress associated with primary hairpin, which results in a peak near $y/h = 0.5$ in Fig. 3c. At the same time, the primary hairpin moves away from the wall with decreasing strength due to viscous diffusion, which results in a diffuse shoulder near $y/h = 0.8$ in Reynolds shears stress profile (Fig. 3c). The maximum observed near the wall at $t^+ = 237$ becomes a larger peak at $t^+ = 395$ because the legs of vortices are strengthened by vortex stretching due to high mean shear.

For relatively low We_τ (= 50), variations of Reynolds shear stress are similar to those in the Newtonian flow. In Fig. 3c, the near-wall peak value of Reynolds shear stress is decreased whereas the profiles are nearly the same as that for

the Newtonian flow in $y/h > 0.6$. This is consistent with the observation in Fig. 1b that vortices becomes fewer in the buffer layer due to inhibition of the auto-generation process by polymer stress but the head of the primary hairpin is unaffected. For larger values of We_τ (≥ 100), the near-wall peaks are significantly suppressed as compared with those in the Newtonian flow. In Fig. 3c, the outer layer bump associated with primary hairpin vortex head disappears, which is observed in the Newtonian and $We_\tau = 50$ flow. The variation of the Reynolds shear stress profiles during the vortex evolution in viscoelastic flow is consistent with DNS or experimental results for fully turbulent drag reduced flows in that reduction of Reynolds shear stress occurs only in the buffer layer for low drag reduction (LDR) while for high drag reduction (HDR), Reynolds shear stress is reduced in the outer layer as well as the inner layer (Li et al., 2006; Ptasinski et al., 2003; Warholic et al., 1999; White and Mungal, 2008).

According to Lumley's criteria of onset of drag reduction, polymers can affect the flow only when the polymer relaxation time is larger than flow time scale (Lumley, 1969). Since the vortex swirling strength is related to the inverse of the vortex time scale, $t_{vortex} \sim 2\pi/\lambda_{ci}$ (Chakraborty et al., 2005), for small We_τ, vortical motions with strong swirling strength ($\lambda_{ci} > 2\pi/We_\tau$) are expected to be affected by polymers. In other words, as We_τ increases, vortices with wider range of swirling strength can be affected by the polymer stress. To see the relationship between polymer relaxation time and vortex swirling strength, the spatio-temporal evolution of the maximum swirling strength in the horizontal plane is shown in Fig. 4 for different We_τ values. Three contour levels of λ_{ci} are shown, over which vortices have smaller time scale than polymer relaxation time for $We_\tau = 50$, 100 and 200, respectively.

For $t^+ < 100$, distributions of $\lambda_{ci,max}$ in the viscoelastic flows are nearly the same as that in the Newtonian flow, which is a result of the formation of Ω-shaped vortex from the initial vortex as shown in Fig. 1. However, viscoelastic effects appear after $t^+ = 100$. In the Newtonian flow (Fig. 4a), large
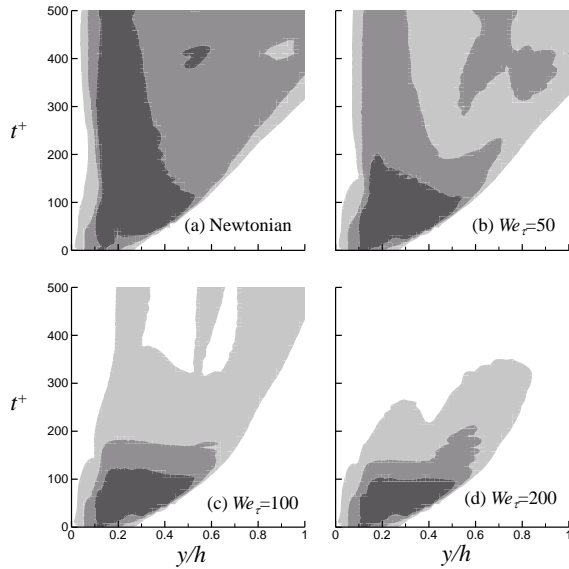
Fig. 4 Spatio-temporal evolution of the maximum swirling strength in the x-z plane $\max(\lambda_{ci})_{xz}$. Three contour levels are shown; $\max(\lambda_{ci})_{xz} = 2\pi/We_\tau$ for $We_\tau = 50$ (dark), 100 (gray) and 200 (light gray).

swirling strength (denoted by dark color) continues to be observed near the wall as time goes by, which is associated with populated vortices generated by auto-generation process. For $We_\tau = 50$ (Fig. 4b), the region in which λ_{ci} larger than $2\pi/We_\tau$ (denoted by dark color) entirely disappears at $t^+ > 200$. For $We_\tau = 100$ and 200, the region in which λ_{ci} is larger than $2\pi/We_\tau$ disappears at $t^+ = 200$ and 300, respectively (Figs 4c and 4d). This suggests that for larger Weissenberg number, vortical motions associated with a wider range of time scales is affected by the polymer stress, consistently with Lumely's time criteria for the onset of drag reduction.

DNS and experimental studies on wall bounded turbulent flows reveal that quasi-streamwise vortices are dominant in the inner layer and hairpin or arch type vortices are dominant in the outer layer (Adrian, 2007; Robinson, 1991). Regarding the strength of the vortices, it has been reported that vortices in the outer layer are weaker than those in the inner layer. In this context, the present results suggest that in viscoelastic flows with small polymer relaxation time but larger than the vortex time scale of the strongest vortices near the wall, near-wall vortices can be affected by the polymer stress whereas weaker vortices in the outer layer remain unaffected. For polymer relaxation times larger than the vortex time scale associated with weak outer vortices, the whole vortices in the flow can be modified and thus flow characteristics in the outer layer as well as inner layer are changed. The interplay between vortex time scale and polymer relaxation time can help explain the differences in the flow characteristics between the low drag reduction regime (LDR) realized for relatively small Weissenberg numbers and the high drag reduction regime (HDR) observed for larger We_τ, e.g. the same slope of mean velocity in log layer for LDR but increased slope for HDR as compared with Newtonian flow (Warholic et al., 1999).

SUMMARY

The effect of dynamical interactions between turbulent vortical structures and polymer stress on turbulent friction drag reduction is examined by performing a series of spectral simulations for channel flow at $Re_\tau = 395$. The initial vortical structure extracted from fully turbulent Newtonian flow is self-consistently evolved in the presence of polymer stresses by utilizing the FENE-P model. For a relatively low Weissenberg number ($We_\tau = 50$) the generation of new vortices is inhibited by polymer-induced counter torques, which results in fewer vortices in the buffer layer. However, the head of primary hairpin is unaffected by the polymer stress. For larger values of We_τ (≥ 100), the hairpin head becomes weaker and vortex auto-generation is almost entirely suppressed. It turns out that as We_τ increases, weaker vortices in the outer layer as well as strong near-wall vortices are affected by the polymer stress.

ACKNOWLEDGEMENT

REFERENCES

Adrian, R. J., 2007, "Hairpin vortex organization in wall turbulence," *Physics of Fluids*, Vol. 19, pp. 041301.

Chakraborty, P., Balachandar, S. and Adrian, R. J., 2005, "On the relationships between local vortex identification schemes," *Journal of Fluid Mechanics*, Vol. 535, pp. 189-214.

Kim, K., Adrian, R. J., Balachandar, S. and Sureshkumar, R., 2008a, "Dynamics of hairpin vortices and polymer-induced turbulent drag reduction," *Physical Review Letters*, Vol. 100, pp. 134504.

Kim, K., Li, C. F., Sureshkumar, R., Balachandar, S. and Adrian, R. J., 2007, "Effects of polymer stresses on eddy structures in drag-reduced turbulent channel flow," *Journal of Fluid Mechanics*, Vol. 584, pp. 281-299.

Kim, K., Sung, H. J. and Adrian, R. J., 2008b, "Effects of background noise on generating coherent packets of hairpin vortices," *Physics of Fluids*, Vol. 20, pp. 105107.

Li, C.-F., Sureshkumar, R. and Khomami, B., 2006, "Influence of rheological parameters on polymer induced turbulent drag reduction," *Journal of Non-Newtonian Fluid Mechanics*, Vol. 140, pp. 23-40.

Lumley, J. L., 1969, "Drag reduction by additives," *Annual Review of Fluid Mechanics*, Vol. 1, pp. 367-384.

Ptasinski, P. K., Boersma, B. J., Nieuwstadt, F. T. M., Hulsen, M. A., Van den Brule, B. and Hunt, J. C. R., 2003, "Turbulent channel flow near maximum drag reduction: simulations, experiments and mechanisms," *Journal of Fluid Mechanics*, Vol. 490, pp. 251-291.

Robinson, S. K., 1991, "Coherent motions in the turbulent boundary layer," *Annual Review of Fluid Mechanics*, Vol. 23, pp. 601-639.

Sureshkumar, R., Beris, A. N. and Handler, R. A., 1997, "Direct numerical simulation of the turbulent channel flow of a polymer solution," *Physics of Fluids*, Vol. 9, pp. 743.

Toms, B. A., 1948. "Some observations on the flow of linear polymer solutions through straight tubes at large Reynolds numbers," *Proc. 1st Int. Congr. Rheol.*, North Holland, Amsterdam.

Toms, B. A., 1977, "On the early experiments on drag reduction by polymers," *Physics of Fluids*, Vol. 20, pp. 3.

Warholic, M. D., Massah, H. and Hanratty, T. J., 1999, "Influence of drag-reducing polymers on turbulence: effects of Reynolds number, concentration and mixing," *Experiments in Fluids*, Vol. 27, pp. 461-472.

White, C. M. and Mungal, M. G., 2008, "Mechanics and Prediction of Turbulent Drag Reduction with Polymer Additives," *Annual Review of Fluid Mechanics*, Vol. 40, pp. 235-256.

Zhou, J., Adrian, R. J., Balachandar, S. and Kendall, T. M., 1999, "Mechanisms for generating coherent packets of hairpin vortices in channel flow," *Journal of Fluid Mechanics*, Vol. 387, pp. 353-396.